



Evaluating the effect of Avastin on breast cancer angiogenesis using synchrotron radiation

Shengmei Gu^{1,2#}, Jingyan Xue^{1,2#}, Yan Xi³, Rongbiao Tang⁴, Wei Jin^{1,2}, Jia-Jian Chen^{1,2}, Xi Zhang^{1,2}, Zhi-Min Shao^{1,2}, Jiong Wu^{1,2,5}

¹Department of Breast Surgery, Fudan University Shanghai Cancer Center, Shanghai 200032, China; ²Department of Oncology, Shanghai Medical College, Fudan University, Shanghai 200032, China; ³School of Biomedical Engineering, School of Life Sciences and Biotechnology, Shanghai Jiao Tong University, Shanghai 200030, China; ⁴Department of Radiology, Ruijin Hospital, School of Medicine, Shanghai Jiao Tong University, Shanghai 200025, China; ⁵Collaborative Innovation Center for Cancer Medicine, Shanghai 200032, China

#These authors contributed equally to this work.

Correspondence to: Jiong Wu. Fudan University Shanghai Cancer Center, 270 Dong An Road, Shanghai 200032, China. Email: wujiong1122@vip.sina.com or shengmei200118@163.com.

Background: The visualization of microvasculature is an essential step in understanding the mechanisms underlying early vessel disorders involved in breast cancer and for developing effective therapeutic strategies. However, generating detailed and reproducible data using immunohistochemistry analysis of breast cancer angiogenesis has been difficult.

Methods: To analyze the diversification of angiogenesis in the development of tumor growth and evaluate the anti-vascular effects of Avastin (bevacizumab), we used new X-ray microangiography and third-generation synchrotron radiation-based micro-computed tomography (SR micro-CT) technology. With these techniques, we were able to investigate the structures and density of microvessels in xenograft mouse models (n=24). Barium sulfate nanoparticles were injected into the left cardiac ventricle of the mice to allow the visualization of blood vessels.

Results: Three-dimensional structures of microvessels were displayed with a high spatial image resolution of 20–30 μm . The density of angiogenesis and the incidence of lung metastasis were significantly reduced in xenograft mouse models of breast cancer treated with Avastin compared with control groups. Also, the density of smaller vessels (diameter <50 μm) was significantly decreased in the Avastin-treated mice, while the density of larger vessels (diameter >100 μm) was not significantly changed.

Conclusions: Avastin inhibited tumor growth and lung metastasis by reducing microvessels. Additionally, synchrotron radiation (SR) techniques are useful as an additional tool for more precise quantification of angiogenesis.

Keywords: Breast cancer; synchrotron radiation (SR); Avastin; microvessel density (MVD); lung metastasis

Submitted Jan 05, 2019. Accepted for publication Mar 09, 2019.

doi: 10.21037/qims.2019.03.09

View this article at: <http://dx.doi.org/10.21037/qims.2019.03.09>

Introduction

According to GLOBOCAN estimates, approximately 12.7 million cancer cases and 7.6 million cancer deaths occurred in 2008. Among these cases, breast cancer is the

leading cause of cancer death among females and affects a more significant number of people worldwide than any other cancer, accounting for approximately 23% of the total number of cancer cases and 14% of cancer deaths (1). Angiogenesis is known to play an essential role in the

growth, progression and metastatic potential of breast cancer (2-6). For these reasons, tumor angiogenesis has become a critical target of breast cancer therapy. New blood vessel formation in the tumor microenvironment is a complicated process that is stimulated by multiple signaling pathways and mediators. Among these mediators, the vascular endothelial growth factor (VEGF) family of ligands play a major role (7,8). Therefore, VEGF has become a promising target of anti-angiogenic therapy, which can be inhibited by preventing VEGF from binding to its receptor or inhibiting signaling downstream of the receptor. Avastin (bevacizumab), a monoclonal antibody that targets all isoforms of VEGF-A, continues to be extensively investigated for the treatment of breast cancer (8,9).

Many studies suggest that VEGF expression is significantly associated with a high intratumoral microvessel density (MVD) and poor prognosis in breast cancer patients (10-13). Vessel normalization is reflected morphologically by a decrease in vessel density as well as loss of branches and a particular laminar vessel organization following anti-angiogenic treatment (14). Currently, the standard used for the evaluation of the angiogenic activity of tumors is the quantification of tumor vascularization from histological tissue sections. Tumor vascularization is typically quantified by determining MVD using immunohistochemical techniques such as staining for CD34, CD31 (PECAM) and von Willebrand factor (vWF) (15,16). However, immunohistochemical methods are relatively subjective, not truly quantitative and only display two-dimensional microvessel structures. Thus, these measurements are not necessarily representative of vascularity throughout the entire tumor (17,18). To address these issues, other researchers have employed automated three-dimensional reconstruction of tumor microvasculature using serial sections. However, several inherent problems resulted from the construction of the three-dimensional structure of tumor microvasculature using serial histological sections, including misalignment, missing sections and imperfect perfusion (17,19-21).

Given these difficulties, we applied X-ray microangiography and third-generation synchrotron radiation-based micro-computed tomography (SR micro-CT) technology to quantify tumor angiogenesis accurately and evaluate the anti-angiogenic effect of Avastin. Synchrotron radiation (SR) techniques present new possibilities for performing numerous types of structural studies. They provide enhanced sensitivity to contrast agents and superior image quality, with a high spatial resolution of 20–30 μm (22). Recently, SR was used as a powerful tool to study small

vessels of various animal organs *ex vivo* and *in vivo* with a high-resolution, high-speed imaging system (22-24). Additionally, breast tumor metastasis to the lung in a xenograft mouse model was imaged using SR, and there were apparent differences observed compared with healthy lung tissue (25,26).

In the present study, we use SR techniques to investigate the diversification of angiogenesis in the development of tumor growth and evaluated the anti-vascular effects of Avastin.

Methods

Cell culture

The highly metastatic MDA-MB-231HM cell line was established by our institute (ZL 200910174455.4). MDA-MB-231HM cells were routinely maintained in Leibovitz's L-15 medium with 2 mM L-glutamine at 37 °C in a humidified atmosphere containing 5% carbon dioxide (CO_2). The medium was supplemented with 10% fetal bovine serum (FBS), 100 U/mL of penicillin and 100 $\mu\text{g/mL}$ of streptomycin.

Tumor model and treatment

Female BALB/c nu/nu mice (20 \pm 2 g, 4–6 weeks) were obtained from the Shanghai Institute of Material Medical, Chinese Academy of Science. All studies on mice were conducted following the NIH Guide for the Care and Use of Laboratory Animals. The study protocol was approved by the Shanghai Medical Experimental Animal Care Committee. Cells (3×10^6) were injected into the mammary fat pads of the mice in a volume of 100 μL . Caliper measurements were performed at 7-day intervals, and tumor volume was calculated as $D \times d^2 \times 0.52$, where D is the long diameter, and d is the short perpendicular diameter. Therapy was initiated on the 8th day after tumor cell injection after the tumor volume had reached approximately 100 mm^3 . A total of 24 animals were randomized to receive injections of either saline, as a control, or Avastin (bevacizumab; Roche, Welwyn Garden City, UK; dose, 7.5 mg/kg) for 3 weeks, twice weekly.

Preparation and injection of contrast agents

Barium sulfate nanoparticles were used as a contrast agent (Sachtleben Chemie GmbH, Germany; size

<700 nanometres) to obtain high-contrast images of microcirculation. The nanoparticles were suspended in glycerol (50% water solution) at a concentration of 0.5 g·mL⁻¹. All animals were anaesthetized via intraperitoneal injection of ketamine (200 mg/kg) (Ketanest; Pfizer, Karlsruhe, Germany). The image contrast agent was then injected into the left ventricle, and the mice were sacrificed before imaging (27).

SR imaging

Tumor microangiography was performed at the Beamline BL13W1, the X-ray imaging and biomedical application station of the Shanghai Synchrotron Radiation Facility (SSRF) in China. When the maximum size of the beam incident to the sample was 47 mm horizontally and 5.2 mm vertically, objects were placed approximately 34 m from the source, and the distance between the samples and the downstream detector varied from 0 cm to 8 m.

SR micro-CT

A monochromatic 37.6 keV X-ray source, just above the K-absorption edge of Barium (37.45 keV), was obtained from the silicon crystals of the Beamline BL13W1. A total of one thousand projections were acquired for each sample, with an exposure time of 25 ms for each projection. The equivalent detector resolution was approximately 9 μm, and the distance from the sample to the detector was 5 cm.

In-line SR phase-contrast imaging

SR phase-contrast imaging was used to observe lung metastases from two groups of mice *in vitro*. The proper imaging parameters used to examine the mouse lung samples were an energy level of 20 keV and an object-to-detector distance of 1 m to obtain the best image quality.

Metastasis assays and immunocytochemistry

At the end of the experiment, trunk blood was collected, and the serum was isolated and analyzed by ELISA for VEGF expression according to the manufacturer's instructions (R&D Systems Inc., Minneapolis, MN, USA). Tumor and lung samples were harvested, and each sample was embedded in paraffin blocks and sectioned at a thickness of 4 μm. Lung sections were stained with hematoxylin and eosin and analyzed using a light microscope (Leica

Instruments, Nussloch, Germany) to detect lung metastases for correlation with SR phase-contrast images. After deparaffinization of the tumor sections, the MVD was detected and quantified as previously reported (28). Briefly, specimens were incubated with an anti-CD34 monoclonal antibody (BioGenex, San Ramon, California, USA) at a dilution of 1:20 or in control, non-immune serum. The reaction products were then incubated with link antibodies, followed by a peroxidase-conjugated streptavidin complex (LSAB kit; DAKO, Carpinteria, CA, USA). Peroxidase activity was visualized using diaminobenzidine tetrahydrochloride solution (DAKO) as the substrate. The sections were lightly counterstained with hematoxylin and then viewed using microscopy. The slide that appeared to have the highest density of microvessels was selected for determination of MVD.

Image processing and statistical analysis

Dr. Yan Xi and Dr. Shengmei Gu conducted image processing and analysis. Image Pro Plus 6.0 (Media Cybernetics Inc., USA) was used to eliminate background noise generated by the detector. SR micro-CT three-dimensional image reconstruction was generated using Amira 4.1 software (Mercury Computer Systems, USA). Quantification and tree analysis of tumor vascularization was performed with the Analyze 10.0 software package (Analyze; Biomedical Imaging Resource, Mayo Foundation, Rochester, MN, USA). Adobe Photoshop CS4 (Adobe Systems Inc., USA) was used to combine the images to construct an overview of the region of interest within the sample.

Analysis of variance and Student's *t*-test were used to determine the statistical significance of differences between the Avastin-treated group and the control group. P values less than 0.05 were considered significant and the confidence intervals quoted were at the 95% level. Statistical analyses were performed with SPSS Software version 13.0 (SPSS, Chicago, IL, USA).

Results

Analysis of angiogenesis using SR micro-CT

After injection of the contrast agent, the mice were euthanized, and the tumor samples were harvested for SR micro-CT imaging. Images of Avastin-treated mice and control mice were obtained after 3 weeks of treatment to quantify the potential anti-angiogenic effect of Avastin.

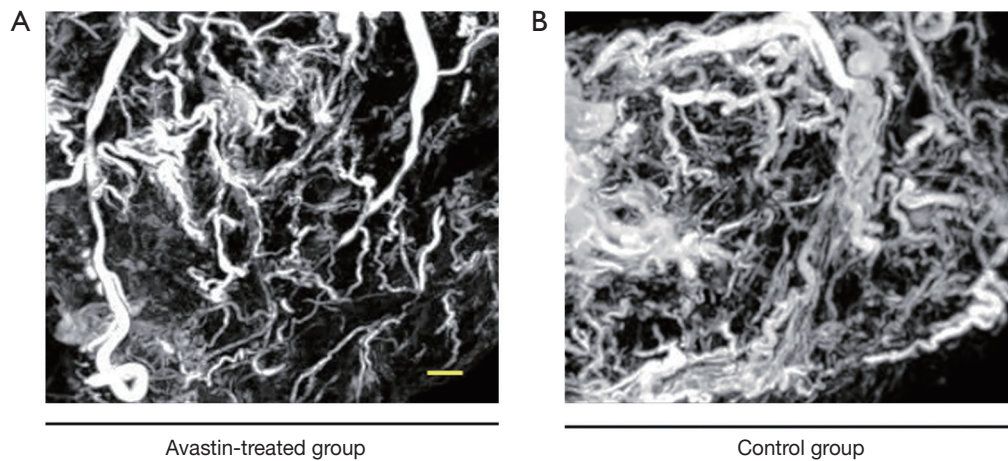


Figure 1 Three-dimensional tumor microvessels of xenograft mouse models *in vitro* by SR Micro-CT. (A) The Avastin-treated group; (B) control group. Minimal vessel diameter is about around 20–30 μm . Bar: 1 mm.

As shown in *Figure 1A,B*, three-dimensional structures of microvessels were displayed with a high spatial image resolution of approximately 20–30 μm . *Figure 2A* shows that quantification of tumor angiogenesis indicated a significant reduction of the MVD in the Avastin-treated group compared to the control group. Also, the density of smaller vessels (diameter <50 μm) was significantly decreased in the Avastin-treated mice, while the density of larger vessels (diameter >100 μm) was not significantly changed. Tree analysis of tumor angiogenesis provided detailed information regarding vascular branches (*Figure 2B,C*). In each group, we chose to analyze the vessel tree with the most branches, and we initiated the tree analysis or branching schematics at the root point. There were 5 branching points and 7 terminal branching vessels in the Avastin-treated group, compared with 23 branching points and 25 terminal branching vessels in the control group, confirming the anti-angiogenesis effect of Avastin.

Histomorphologic analysis

The vascularization of tumors derived from the Avastin-treated and untreated breast cancer xenograft models was analyzed by staining vessels with CD34 (*Figure 3A,B*). Quantitative analysis indicated a lower tumor vascular density in the Avastin-treated group compared to the control group. This was consistent with the vascular evaluation of breast cancer tissue in the Avastin-treated group and control group by SR micro-CT using barium sulfate nanoparticles as a contrast agent.

Tumor volume and lung metastasis analysis

In the following experiments, we assessed the effect of Avastin on tumor growth and metastasis using orthotopic xenograft tumor models in athymic mice. Tumor growth was analyzed at the indicated time intervals. The results revealed that the tumor volume was significantly lower in mice treated with Avastin (*Figure 4A*). Also, we measured the amount of VEGF in the serum of the mice using ELISA. The level of VEGF was significantly lower in the serum of mice from the Avastin-treated group compared to the control group (*Figure 4B*).

To study pulmonary metastasis influenced by Avastin, lungs from mice in the Avastin-treated group and control group (*Figure 5*) were examined physically by SR phase-contrast imaging *in vitro* and then subjected to microscopic examination to detect morphologic evidence of tumor cells via light microscopy of H&E-stained paraffin sections. As shown in *Figure 5*, the incidence of lung metastasis was decreased in mice treated with Avastin compared with the control group.

Discussion

This study aimed to assess the feasibility of the SR techniques for use in angiography applications in xenograft mouse models of breast cancer and, most importantly, to evaluate the effect of Avastin on tumor angiogenesis and lung metastasis. Detailed visualization of the vascular

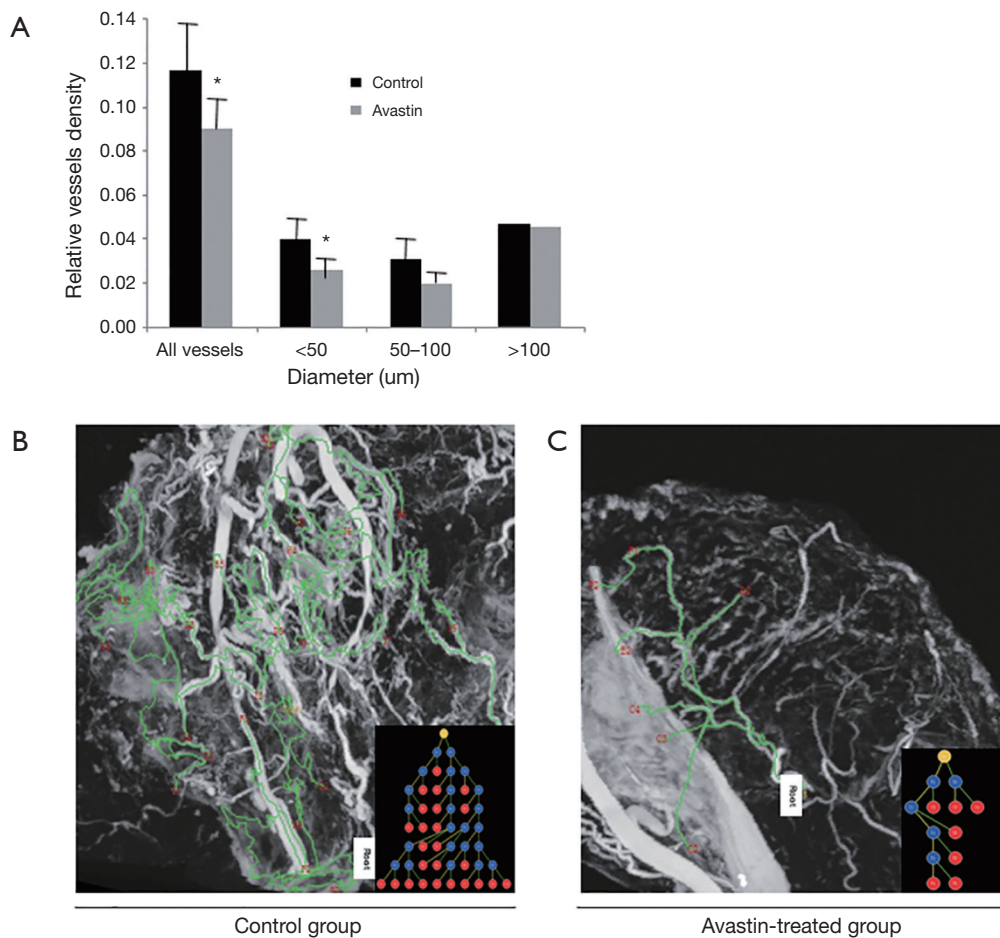


Figure 2 Vessels density of Avastin-treated group and control group. (A) Relative vessels density analysis of Avastin-treated group and control group. *, $P < 0.05$ versus control. Vascular tree analysis of the two groups: (B) control group ($n=6$); (C) Avastin-treated group ($n=6$). The vessel trees that had the most branches were analyzed in the two groups, and the tree analysis or branching schematics was started at the root point.

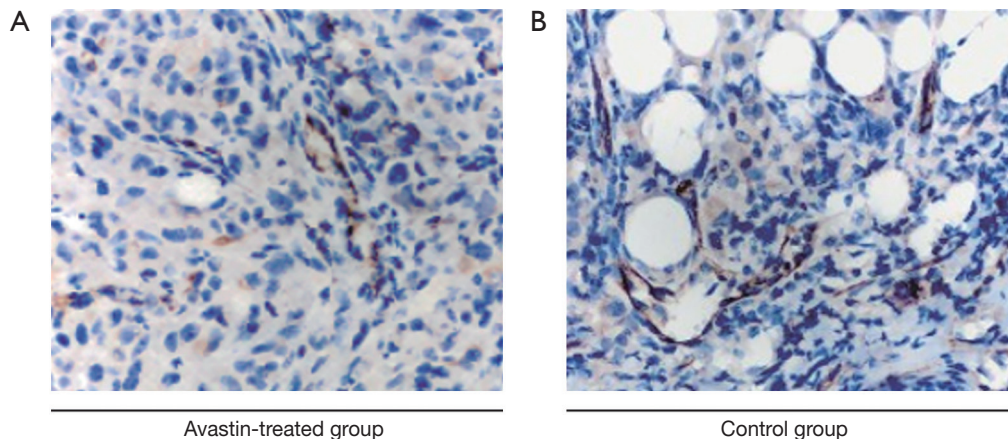


Figure 3 Immunohistochemical images of xenograft mouse models of breast cancer by CD34 staining. (A) Avastin-treated group ($n=6$); (B) control group ($n=6$). Original magnification $\times 400$.

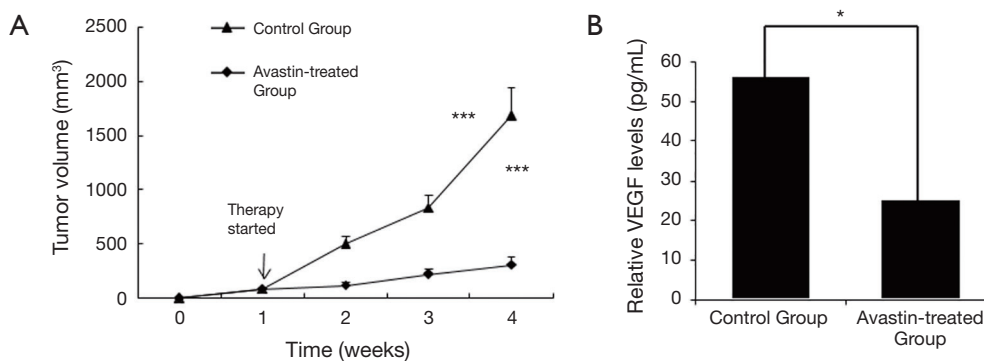


Figure 4 Tumor growth and VEGF analysis of Avastin-treated group and control group. (A) Avastin inhibits MDA-MB-231HM tumor growth. Treatment with saline control (n=12) or Avastin (n=12), was initiated in established tumors (100 mm³) on day 8 post tumor cell injection and continued for three weeks. Tumor volume was measured once a week. Points, mean tumor volume; ***, P<0.0001, treatment versus control. (B) Measurement of the amounts of VEGF in the mice serum by ELISA. The level of VEGF was significantly lower in the serum from Avastin-treated group when compared to the control group. *, P<0.05 versus control. VEGF, vascular endothelial growth factor.

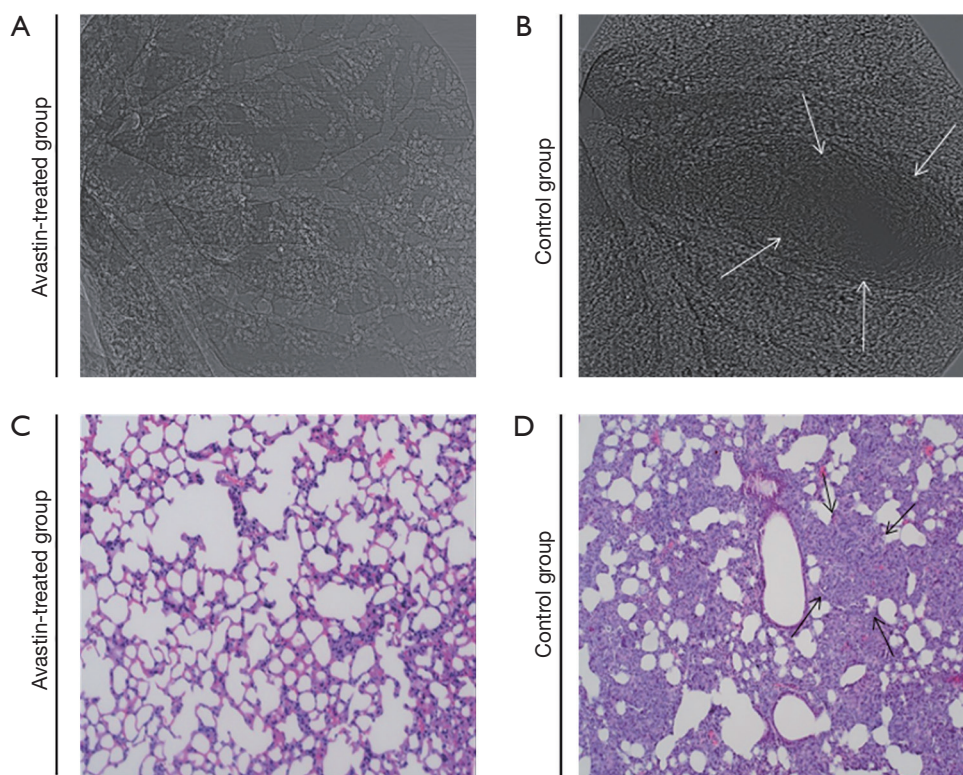


Figure 5 Pulmonary metastasis analysis. SR phase-contrast imaging (A,B) was obtained at 20 keV with the object-to-detector distance of 1 m. The pixel size was 9 μm × 9 μm; the exposure time was 2.5 ms. (C,D), H&E-stained examination was carried *in vitro*. Original magnification ×200. The arrows in (B) and (D) indicated lung metastasis. Avastin-treated group (n=12), control group (n=12).

systems of tumors and lung metastases was demonstrated. Previous studies have described the capability to quantitatively analyze MVD, vessel distribution patterns

and connectivity using SR (22,29-31). However, this high-resolution technology has not been used to evaluate the anti-angiogenesis properties and inhibition of lung

metastasis by Avastin before the present study.

It has been demonstrated that VEGF increases vascular permeability, facilitates EC migration (7) and remodels the ECM (32,33). Avastin binds human VEGF and prevents activation of VEGFR1 and VEGFR2 to restrain EC sprouting. Anti-angiogenic treatment has a relatively more significant effect on smaller vasculature compared to other types of the vasculature (17,34-37). Reduced and fortified tumor vasculature may also inhibit the shedding of cancer cells into the circulation, which is a prerequisite for metastasis (14). In previous studies, tumor vascularization was quantified by determining MVD using immunohistochemical techniques such as staining for CD34, CD31 (PECAM) and vWF (15,16). However, these methods are relatively subjective, which only show two-dimensional microvessel structures, and cannot truly quantify the vascularity throughout the entire tumor to evaluate the effect of Avastin on breast cancer angiogenesis (17,18). In this study, the effects of Avastin treatment, assessed by SR, were not only in line with previous reports but also provided more quantitative information. The construction of the three-dimensional structure of tumor microvasculature was well displayed in *Figure 2*. Furthermore, the relative vessels density results were showed to confirm the anti-angiogenesis effect of Avastin.

Compared with other techniques for tumor vessel morphologic evaluation and measurement of vessel content, SR micro-CT has several additional features. It provides the opportunity to study the three-dimensional structures involved in tumor angiogenesis, such as vascular connectivity, angles, and branches. SR can also be used to image an entire organ and, hence, can be a useful tool for performing quantitative measurements of intrapulmonary tumors and their vascular content in breast carcinoma-bearing mouse models showing high lung metastasis rates. Also, the spatial resolution of SR vascular imaging, after filling samples with barium sulfate nanoparticles, can reach approximately 10 μm , which is much higher than that of conventional angiography techniques, such as CT, MRI, and ultrasound (16,23,25,38-40). Also, barium sulfate nanoparticles are very stable and seldom diffuse from blood vessels to the surrounding tissue. However, these nanoparticles can potentially cause serious side effects, and mice may die in a short time after that injection.

Nevertheless, given the high spatial resolution required for vascular imaging, observation of microvessels *in vivo* without contrast agents is challenging. Iodine has been used as a contrast agent in some studies to obtain vascular images in real time. However, it can rapidly diffuse, and thus, it

cannot be used to observe blood vessels for long periods (22).

In conclusion, this study uses SR imaging, specifically SR micro-CT imaging, as an ideal modality to assess the effects of anti-angiogenic therapy and visualize pulmonary metastasis in xenograft mouse models of breast cancer following Avastin treatment. Most importantly, the detailed quantitative information obtained from SR-based microangiography indicates a new direction for the application of anti-angiogenic Avastin therapy in basic and clinical cancer research. Although SR is a promising new imaging tool for the analysis of tumor progression and therapeutic drug responses, due to the operational complexity of this technology, it is difficult to detect in large quantities.

Acknowledgements

This work was performed at the Beamline BL13W X-ray imaging and biomedical application station of the Shanghai Synchrotron Radiation Facility (SSRF) in China.

Funding: This work was supported by the National Basic Research Program of China (973 Program 2010CB834305) and National Natural Science Foundation of China (NSFC) (81602324 to J Xue).

Footnote

Conflicts of Interest: The authors have no conflicts of interest to declare.

Ethical Statement: The study protocol was approved by the Shanghai Medical Experimental Animal Care Committee.

References

1. Torre LA, Bray F, Siegel RL, Ferlay J, Lortet-Tieulent J, Jemal A. Global cancer statistics, 2012. *CA Cancer J Clin* 2015;65:87-108.
2. Wu FT, Man S, Xu P, Chow A, Paez-Ribes M, Lee CR, Pirie-Shepherd SR, Emmenegger U, Kerbel RS. Efficacy of Cotargeting Angiopoietin-2 and the VEGF Pathway in the Adjuvant Postsurgical Setting for Early Breast, Colorectal, and Renal Cancers. *Cancer Res* 2016;76:6988-7000.
3. Uzzan B, Nicolas P, Cucherat M, Perret GY. Microvessel density as a prognostic factor in women with breast cancer: a systematic review of the literature and meta-analysis. *Cancer Res* 2004;64:2941-55.
4. Weidner N, Folkman J, Pozza F, Bevilacqua P, Allred EN, Moore DH, Meli S, Gasparini G. Tumor angiogenesis:

- a new significant and independent prognostic indicator in early-stage breast carcinoma. *J Natl Cancer Inst* 1992;84:1875-87.
5. Buxton IL, Yokdang N, Matz RM. Purinergic mechanisms in breast cancer support intravasation, extravasation and angiogenesis. *Cancer Lett* 2010;291:131-41.
 6. Kraby MR, Opdahl S, Akslen LA, Bofin AM. Quantifying tumour vascularity in non-luminal breast cancers. *J Clin Pathol* 2017;70:766-74.
 7. Hicklin DJ, Ellis LM. Role of the vascular endothelial growth factor pathway in tumor growth and angiogenesis. *J Clin Oncol* 2005;23:1011-27.
 8. Damasceno M. Bevacizumab for the first-line treatment of human epidermal growth factor receptor 2-negative advanced breast cancer. *Curr Opin Oncol* 2011;23 Suppl:S3-9.
 9. Redondo A, Ramos Vazquez M, Manso L, Gil Gil MJ, Garau Llinas I, Garcia-Garre E, Rodriguez CA, Chacon JI, Lopez-Vivanco G. Long-term response to first-line bevacizumab-based therapy in patients with metastatic breast cancer: results of the observational "LORENA" study. *Onco Targets Ther* 2018;11:5845-52.
 10. Toi M, Hoshina S, Takayanagi T, Tominaga T. Association of vascular endothelial growth factor expression with tumor angiogenesis and with early relapse in primary breast cancer. *Jpn J Cancer Res* 1994;85:1045-9.
 11. Chhieng DC, Tabbara SO, Marley EF, Talley LI, Frost AR. Microvessel density and vascular endothelial growth factor expression in infiltrating lobular mammary carcinoma. *Breast J* 2003;9:200-7.
 12. Welsh SJ, Bellamy WT, Briehl MM, Powis G. The redox protein thioredoxin-1 (Trx-1) increases hypoxia-inducible factor 1alpha protein expression: Trx-1 overexpression results in increased vascular endothelial growth factor production and enhanced tumor angiogenesis. *Cancer Res* 2002;62:5089-95.
 13. Bolat F, Kayaselcuk F, Nursal TZ, Yagmurdu MC, Bal N, Demirhan B. Microvessel density, VEGF expression, and tumor-associated macrophages in breast tumors: correlations with prognostic parameters. *J Exp Clin Cancer Res* 2006;25:365-72.
 14. Jain RK. Normalization of tumor vasculature: an emerging concept in antiangiogenic therapy. *Science* 2005;307:58-62.
 15. Fanelli M, Locopo N, Gattuso D, Gasparini G. Assessment of tumor vascularization: immunohistochemical and non-invasive methods. *International Journal of Biological Markers* 1999;14:218-31.
 16. McDonald DM, Choyke PL. Imaging of angiogenesis: from microscope to clinic. *Nat Med* 2003;9:713-25.
 17. Savai R, Langheinrich AC, Schermuly RT, Pullamsetti SS, Dumitrescu R, Traupe H, Rau WS, Seeger W, Grimminger F, Banat GA. Evaluation of angiogenesis using micro-computed tomography in a xenograft mouse model of lung cancer. *Neoplasia* 2009;11:48-56.
 18. Bernsen MR, Kooiman K, Segbers M, van Leeuwen FW, de Jong M. Biomarkers in preclinical cancer imaging. *Eur J Nucl Med Mol Imaging* 2015;42:579-96.
 19. Guo L, Burke P, Lo SH, Gandour-Edwards R, Lau D. Quantitative analysis of angiogenesis using confocal laser scanning microscopy. *Angiogenesis* 2001;4:187-91.
 20. Itoh J, Kawai K, Serizawa A, Yasumura K, Ogawa K, Osamura RY. A new approach to three-dimensional reconstructed imaging of hormone-secreting cells and their microvessel environments in rat pituitary glands by confocal laser scanning microscopy. *J Histochem Cytochem* 2000;48:569-78.
 21. Zagorchev L, Mulligan-Kehoe MJ. Molecular imaging of vessels in mouse models of disease. *Eur J Radiol* 2009;70:305-11.
 22. Liu P, Sun J, Zhao J, Liu X, Gu X, Li J, Xiao T, Xu LX. Microvascular imaging using synchrotron radiation. *J Synchrotron Radiat* 2010;17:517-21.
 23. Shirai M, Schwenke DO, Eppel GA, Evans RG, Edgley AJ, Tsuchimochi H, Umetani K, Pearson JT. Synchrotron-based angiography for investigation of the regulation of vasomotor function in the microcirculation in vivo. *Clin Exp Pharmacol Physiol* 2009;36:107-16.
 24. Shirai M, Schwenke DO, Tsuchimochi H, Umetani K, Yagi N, Pearson JT. Synchrotron radiation imaging for advancing our understanding of cardiovascular function. *Circ Res* 2013;112:209-21.
 25. Liu X, Zhao J, Sun J, Gu X, Xiao T, Liu P, Xu LX. Lung cancer and angiogenesis imaging using synchrotron radiation. *Phys Med Biol* 2010;55:2399-409.
 26. Zhang M, Peng G, Sun D, Xie Y, Xia J, Long H, Hu K, Xiao B. Synchrotron radiation imaging is a powerful tool to image brain microvasculature. *Med Phys* 2014;41:031907.
 27. Jin W, Chen BB, Li JY, Zhu H, Huang M, Gu SM, Wang QQ, Chen JY, Yu S, Wu J, Shao ZM. TIEG1 inhibits breast cancer invasion and metastasis by inhibition of epidermal growth factor receptor (EGFR) transcription and the EGFR signaling pathway. *Mol Cell Biol* 2012;32:50-63.
 28. Chen CN, Cheng YM, Liang JT, Lee PH, Hsieh FJ, Yuan

- RH, Wang SM, Chang MF, Chang KJ. Color Doppler vascularity index can predict distant metastasis and survival in colon cancer patients. *Cancer Res* 2000;60:2892-7.
29. Lu W, Dong Z, Liu Z, Fu W, Peng Y, Chen S, Xiao T, Xie H, Du G, Deng B, Zhang X. Detection of microvasculature in rat hind limb using synchrotron radiation. *J Surg Res* 2010;164:e193-9.
 30. Yamashita T. Evaluation of the microangioarchitecture of tumors by use of monochromatic x-rays. *Invest Radiol* 2001;36:713-20.
 31. Zhang MQ, Sun DN, Xie YY, Peng GY, Xia J, Long HY, Xiao B. Three-dimensional visualization of rat brain microvasculature following permanent focal ischaemia by synchrotron radiation. *Br J Radiol* 2014;87:20130670.
 32. Mantzaris NV, Webb S, Othmer HG. Mathematical modeling of tumor-induced angiogenesis. *J Math Biol* 2004;49:111-87.
 33. Hwang-Bo J, Bae MG, Park JH, Chung IS. 3-O-Acetyloleonic acid inhibits VEGF-A-induced lymphangiogenesis and lymph node metastasis in an oral cancer sentinel lymph node animal model. *BMC Cancer* 2018;18:714.
 34. Benjamin LE, Golijanin D, Itin A, Pode D, Keshet E. Selective ablation of immature blood vessels in established human tumors follows vascular endothelial growth factor withdrawal. *J Clin Invest* 1999;103:159-65.
 35. Gee MS, Procopio WN, Makonnen S, Feldman MD, Yeilding NM, Lee WM. Tumor vessel development and maturation impose limits on the effectiveness of anti-vascular therapy. *Am J Pathol* 2003;162:183-93.
 36. Ferrara N, Kerbel RS. Angiogenesis as a therapeutic target. *Nature* 2005;438:967-74.
 37. Wang N, Jain RK, Batchelor TT. New Directions in Anti-Angiogenic Therapy for Glioblastoma. *Neurotherapeutics* 2017;14:321-32.
 38. Fink C, Kiessling F, Bock M, Lichy MP, Misselwitz B, Peschke P, Fusenig NE, Grobholz R, Delorme S. High-resolution three-dimensional MR angiography of rodent tumors: morphologic characterization of intratumoral vasculature. *J Magn Reson Imaging* 2003;18:59-65.
 39. Cai W, Gambhir SS, Chen X. Chapter 7. Molecular imaging of tumor vasculature. *Methods Enzymol* 2008;445:141-76.
 40. Cebulla J, Kim E, Rhie K, Zhang J, Pathak AP. Multiscale and multi-modality visualization of angiogenesis in a human breast cancer model. *Angiogenesis* 2014;17:695-709.

Cite this article as: Gu S, Xue J, Xi Y, Tang R, Jin W, Chen JJ, Zhang X, Shao ZM, Wu J. Evaluating the effect of Avastin on breast cancer angiogenesis using synchrotron radiation. *Quant Imaging Med Surg* 2019;9(3):418-426. doi: 10.21037/qims.2019.03.09